DOI:10.22337/2587-9618-2025-21-1-202-221

LONGITUDINAL DEFORMATIONS OF SHORTENING OF STEEL-REINFORCED CONCRETE STRUCTURES UNDER COMPRESSION FROM SHORT-TERM LOADS

Denis V. Konin

TSNIISK named after V. A. Koucherenko JSC Research Center of Construction, Moscow, RUSSIA

Abstract: Determination and investigation of longitudinal deformations of shortening of steel-reinforced concrete structures is an important step in the calculation of complex spatial schemes of buildings. Ignoring these deformations can make it difficult to operate the facility and, in some cases, lead to the failure of adjacent structures. The study of longitudinal deformations of shortening of steel-reinforced concrete structures has not been given due attention before. The longitudinal deformations of shortening for steel-reinforced concrete compressed elements using a large range of heavy concretes (from B25 to B80) and percentages of reinforcement (from 0 to 22%) are estimated. The deformations were calculated. The analysis of experimental data obtained during testing of conditionally centrally compressed models of columns of steel-reinforced concrete structures is presented. It is shown that the existing diagrams of concrete work do not accurately describe the work of a composite steel-reinforced concrete structure, it is its shortening and reduced rigidity. When the structure is compressed, concrete loses its destruction at earlier stages of loading than it would be for concrete or reinforced concrete. This fact is caused by the stress-strain state of the concrete section separated by steel elements, as well as the effects of early detachment and slippage along the «steel-concrete» contact surface. It is necessary to use a system of additional coefficients to eliminate the established discrepancy in determining the magnitude of longitudinal deformation (shortening) under the action of short-term loads and experimentally obtained data. These coefficients should increase the theoretical value of the expected relative deformations and consider the features of the work of conventional and high-strength concrete as part of compressible steel-reinforced concrete structures. When determining the stiffness values for steel-reinforced concrete structures under the action of short-term loads and bringing the calculated longitudinal stiffness to a value close to experimental data, it is proposed to introduce an additional coefficient. This coefficient further reduces the longitudinal rigidity of the structure depending on the stress level in concrete and steel.

Keywords: central compression, off-center compression, vertical deformation, longitudinal stiffness, steel-reinforced concrete structure, column, high-rise building

ПРОДОЛЬНЫЕ ДЕФОРМАЦИИ УКОРОЧЕНИЯ СТАЛЕЖЕЛЕЗОБЕТОННЫХ КОНСТРУКЦИЙ ПРИ СЖАТИИ ОТ НЕПРОДОЛЖИТЕЛЬНЫХ НАГРУЗОК

Д.В. Конин

ЦНИИСК им. В.А. Кучеренко АО «НИЦ «Строительство», г. Москва, РОССИЯ

Аннотация: Определение и исследование продольных деформаций укорочения сталежелезобетонных конструкций является важным этапом в вопросе расчета сложных пространственных схем зданий, поскольку их игнорирование может затруднить эксплуатацию объекта и, в некоторых случаях, привести к выходу из строя примыкающих конструкций. Ранее исследованию продольных деформаций укорочения сталежелезобетонных конструкций не уделялось должного внимания. Дана оценка продольных деформаций укорочения для сталежелезобетонных сжатых элементов с применением большого диапазона тяжелых бетонов (от B25 до B80) и процентов армирования (от 0 до 22%), произведен расчет деформаций. Представлен анализ экспериментальных данных, полученных при испытании условно центрально сжатых моделей колонн сталежелезобетонных конструкций. Показано, что существующие диаграммы работы бетона не вполне точно описывают работу составной сталежелезобетонной конструкции, в частности, ее укорочение и приведенную жесткость. При работе конструкции на сжатие бетон теряет разрушается на более ранних этапах нагружения, чем это было бы для бетона или железобетона. Этот факт вызван напряженно-деформированным состоянием разделенного стальными элементами бетонного сечения, а также эффектами раннего отслоения и проскальзывания по контактной поверхности «сталь-бетон». Для того, чтобы устранить установленное разночтение в определении величины продольной деформации (укорочения) при действии кратковременных нагрузок и экспериментально полученных данных, необходимо использовать систему дополнительных коэффициентов, которые должны увеличивать теоретическую величину ожидаемых относительных деформаций, а также должны учитывать особенности работы бетонов обычной и высокой прочности в составе сжимаемых сталежелезобетонных конструкций. При определении значений жесткостей для сталежелезобетонных конструкций под действием кратковременных нагрузок и приведении расчетной продольной жесткости к величине, близкой к экспериментальным данным, предложено ввести дополнительный коэффициент, который дополнительно понижает продольную жесткость конструкции в зависимости от уровня напряжений в бетоне и стали.

Ключевые слова: центральное сжатие, внецентренное сжатие, вертикальная деформация, продольная жесткость, сталежелезобетонная конструкция, колонна, высотное здание

INTRODUCTION

The columns of high-rise buildings and the supporting structures of stadium coverings, where the elements are subjected to significant compression forces, are usually designed in steel-reinforced concrete structures, in particular, columns with rigid reinforcement. For correct analysis of complex spatial schemes of buildings, it is extremely important to correctly determine the longitudinal deformations of steel-reinforced concrete structures. Despite the fact that the current normative documents on analysis and design of such structures SP 63.13330 “Concrete and Reinforced Concrete Structures”, SP 267.1325800 “Buildings and High-Rise Complexes...”, SP 266. 1325800 “Steel-reinforced concrete structures...” do not regulate the ultimate values of shortening for eccentrically compressed elements. Ignoring these deformations can complicate the operation of the facility and in some cases lead to the failure of adjacent structures. The effect of longitudinal deformations in multi-storey and high-rise buildings can result in misalignment of the vertical cells of the frame, which should have deformations no greater than those specified in clause D.1.9 of SP 20.13330 and clause 8.2.4.16 of SP 267.1325800 “Buildings and high-rise complexes...” where the allowed displacements are of 1/300 of the floor height and less.

Cells skew is calculated by the formula f1/hs + f2/l, where f1 and f2 are horizontal and vertical displacements respectively, and hs and l - cell height and its span as can be seen from Figure E.3 in SP 20.13330 “Loads and Actions". In addition, during construction and operation of high-rise buildings the standards GOST 27751-2014 “Reliability of building structures and foundations. Main provisions” and GOST 31937-2011 ”Buildings and structures. Rules for inspection and monitoring of technical condition” stipulate monitoring of deformations of structures.

Shear deformations of the frame cell can cause damage to the exterior structural components, facade modules, partition walls. It can also impede the operation of elevators. The drift of the top of the building from the vertical, as well as standard formulas for cell deformation only regulate the slab shear relative to each other and do not include estimates of potential additional vertical deformation. For example, damage can also occur in high-rise and multi-floor buildings due to varying column shortening. In the U.S. structural design codes [1, 19], the shortening effect is accounted for by the so-called Drift Measurement Index (DMI = Drift Measurement Index) for high-rise structures. This value is essentially the average shear deformation of a vertical rectangular cell. Its influence on envelope structures for their main types is taken with regard to [2].

It is obvious that in the absence of experimentally and theoretically substantiated methodology for calculation of vertical longitudinal deformations of complex composite steel reinforced concrete structures almost impossible to reliably determine the values of controlled vertical deformations of the entire building frame and its structural components, misalignments of frame cells, which are permissible for a particular facility. For large-span structures, correct determination of longitudinal deformations of steel- reinforced concrete support structures guarantee normal operation of coverings and grandstand structures resting on them.

The papers [3, 4] demonstrate the results of tests of eccentrically compressed steel-reinforced concrete elements with a ratio of longitudinal reinforcement from 3 to 20 percent. The elements are made of concrete with compressive strength class up to B90 and fiber-reinforced concrete. In these articles, as well as in [5], devoted to the calculation of columns for oblique eccentric compression, the test results and calculations for the ultimate limit states are presented in detail.

The design of frames of unique buildings and structures with steel-reinforced concrete elements is based on the use of certified software systems that implement the finite element method. Columns and supports of these structures, as a rule, are modeled as bars of reduced stiffness, or as a "combined" design by solid elements (separately steel, separately concrete and rebars), combined by common nodes. Such models, even in calculations with respect to nonlinear deformation diagrams of steel and reinforced concrete, cannot fully account for the behavior of the composite structure, in particular, the possibility of slippage of concrete relative to the steel core [4].

The review of experimental studies in Russia and the world and normative documents [6, 13] shows that earlier the issue of studying longitudinal shortening deformations of steel-reinforced concrete structures was not paid proper attention to. In contrast to long-term shortening due to creep and shrinkage of concrete [14, 15, 16, 19, 20, 21], which have been extensively studied in recent years, the regularities of deformations of steel-reinforced-concrete structures under short-term loads are poorly studied.

RESEARCH METHODS

The laboratories of the V.A. Kucherenko Central Research Institute of Steel and Concrete Structures have carried out large-scale tests of steel-reinforced concrete structures for central and off-centered compression. Detailed test results are given in [3, 4]. The paper [7] provides a methodology for calculating the strength of steel reinforced concrete compression-bending elements (columns) using a nonlinear deformation model, which corresponds to the current standards for the analysis of reinforced concrete structures such as SP 63.13330. The ultimate limit state of the structure is determined by reaching the ultimate longitudinal strains of concrete, reinforcement and rigid reinforcing steel. The ultimate value of longitudinal strains of concrete $\varepsilon_{b,ult}$ is accepted depending on the ratio of concrete edge strains ε_1 and ε_2 by linear interpolation from -0.002 at $\varepsilon_1/\varepsilon_2=1$ to -0.0035 at $\varepsilon_1/\varepsilon_2\leq 0$, where ε_2 is the concrete strain at the most compressed edge with the minus sign. In this case, the strength of the tensile concrete is not accounted for in the calculation. The ultimate value of the strain of the steel of the core and tensile reinforcement is assumed to be 0.025 for central and eccentric compression.

In actual norms for the calculation of steel structures SP 16.13330 "Steel structures" a generalized diagram of steel deformation under load action is given for different steels. Clause 4.2.4 establishes the possibility of modeling of nonlinear operation of steel according to the diagram of Figure B.1 and Table B.9 in SP 16.13330.2017. Figure 1a,b shows stress vs. strain relationships for steels from C255 to C550 in accordance with the normative parameters. The ultimate strain of steel should be taken corresponding to the end of the yield plane. For steels with yield strengths from 255 to 550 MPa, the value of the ultimate strain will vary from 0.017 to 0.047 respectively. In this connection, it is obvious that it is incorrect to take the ultimate strain as 0.025 as for reinforcing steel, regardless of the yield strength of the steel. Since for steels C235, C245, C255 this value will correspond to the steel performance in the self-strengthening region above the yield point, and for C355 and above the plastic properties of the steel will not be fully utilized. It is important to note that ignoring the performance of steel in the elastic-plastic deformation region in calculations using a two-line diagram of steel performance (the so-called "Prandtl diagram") can lead to a distorted picture of strain distribution in the cross-section of the steel-reinforced concrete element and inaccurate results of the shortening calculation.

In order to properly account for concrete strains in steel and reinforced concrete structures, several variants of diagrams of behavior under load can be adopted. In recent standards it is allowed to use two- and three-line diagrams (clauses 6.1.19...6.1.21 in SP 63.13330), as well as curvilinear diagram of concrete deformation (Appendix G in SP 63.13330), which is developed on the basis of the works summarized in the monograph by Academician N.I. Karpenko [8, 12, 16]. Also, Prof. G.V. Murashkin and co-authors developed and presented in [9, 10] an exponential version of the concrete deformation diagram. In addition to those listed above, it is possible to use the curvilinear diagram given in the European Union standards (Eurocode 2). In the present work we will limit ourselves to consideration of three-line diagrams (Figure 1 c) and curvilinear diagrams (Figure 1 d), since by now they are reflected in normative documents, implemented in finite element program complexes, tested by a large number of experimental data and many years of experience in design and operation of real buildings and structures.

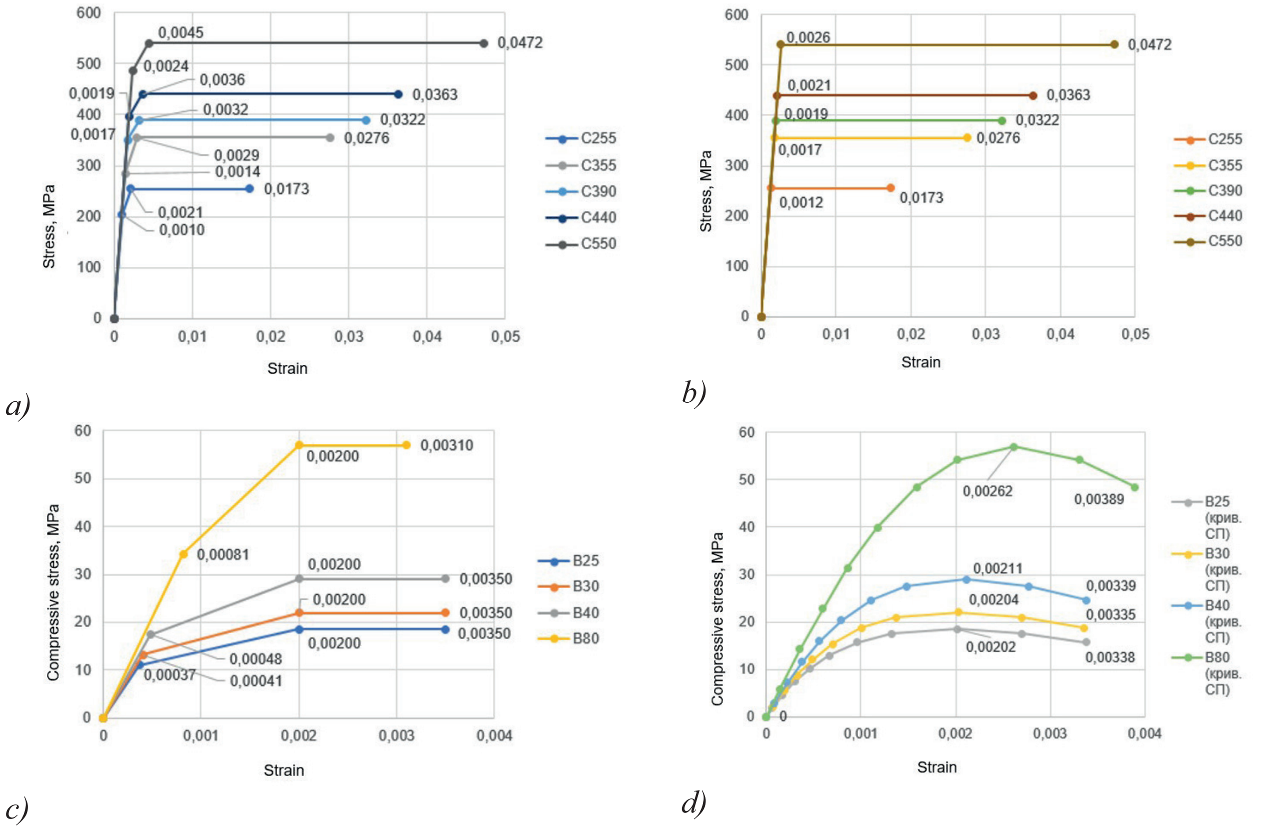

Figure 1. Deformation diagrams for steel and concrete: a - three-linear for steel (S3L), b - bilinear for steel (S2L), c - three-linear for concrete according to SP 63.13330 (B3L), d - curvilinear for concrete according to SP 63.13330 (BCL)

Calculation of theoretical longitudinal deformations of a bar subjected to compression without moments is carried out in the following way to construct theoretical curves. At the break points of each diagram, the boundaries of the loading stages (I, II, III...) are drawn, within which the shortenings of the structure are calculated. Thus, Figure 2 shows an example of splitting two- and three-line diagrams into stages for concrete B80 and steel C255, Figure 3 shows an example of splitting a curvilinear diagram of concrete B80 with a three-linear diagram of steel C255 performance. The longitudinal deformation of the bar at the first (I) Δl_I and subsequent stages (II, III, ...) and the total longitudinal deformation (shortening) ΔL are calculated as follows:

$$\Delta l_{I,\ II,\ III\ldots} = \Delta\varepsilon_{I,\ II,\ III\ldots}\, L,$$
$$\Delta L = \sum_{m=I}^{VIII} \Delta l_m \quad (1)$$

where L is the effective design length of the bar, $\Delta\varepsilon_{I,\ II,\ III\ldots}$ is the range of strain on the considered section of the diagram.

For each stage, the corresponding moduli of deformation for steel, concrete, and reinforcement are determined. For stage I, these moduli will be denoted as $E_{st,I}, E_{b,I}, E_{s,I}$ respectively. For each stage of the steel-reinforced concrete structure, the concrete reduction factors are calculated, and then the area of the reduced section A_{red}, the longitudinal stiffness of the reduced section within the stage ΔD_a using stage I as an example is calculated by the formula:

$$\alpha_{st,I} = \frac{E_{st,I}}{E_{b,I}}, \alpha_{s,I} = \frac{E_{s,I}}{E_{b,I}}, \quad (2)$$
$$A_{red,I} = A_b + A_{st}\alpha_{st,I} + A_s\alpha_{s,I} \quad (3)$$
$$\Delta D_{a,I} = E_{b,I} A_{red,I} \quad (4)$$

where A_b, A_{st}, A_s are the areas of concrete cross-section, steel core cross-section and rebars' cross-section respectively. The increments of longitudinal force ΔN up to the corresponding strain stage boundaries and the limiting value of longitudinal force N at which the strain increases without increasing the load are calculated using the formulas:

$$\Delta N_I = \Delta\varepsilon_I\, \Delta D_{a.I}\ ,\ N = \sum_{m=I}^{VIII} \Delta N_m \quad (5)$$

By performing calculations using the above formulas allows us to estimate the value of shortening in compression and compare it with the corresponding results of numerical modeling and experimental data.

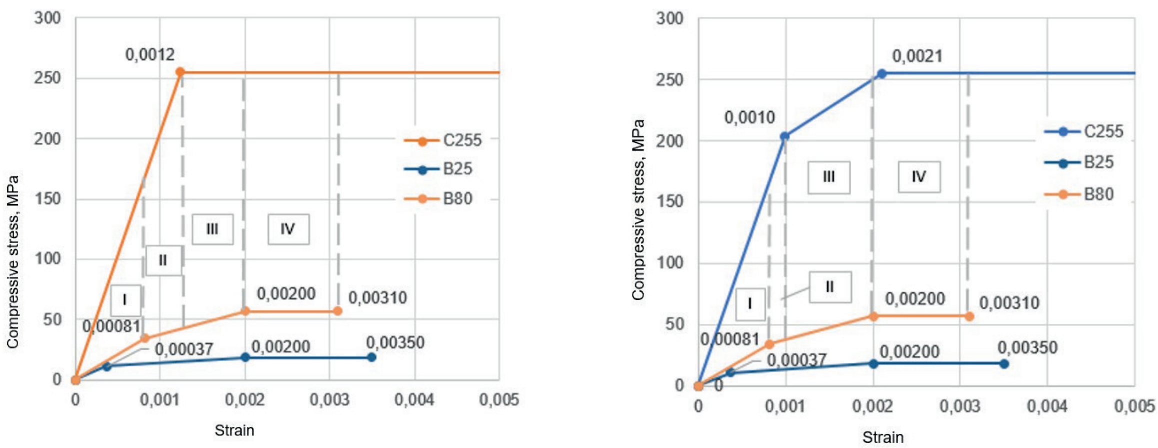

a) *b)*

<u>Figure 2.</u> To the description of the stages of performance of steel-reinforced concrete compressed bar: a - superposition of two-line diagram of steel and three-line diagram of concrete (S2L+B3L), b - superposition of three-line diagrams of steel and concrete (S3L+B3L).

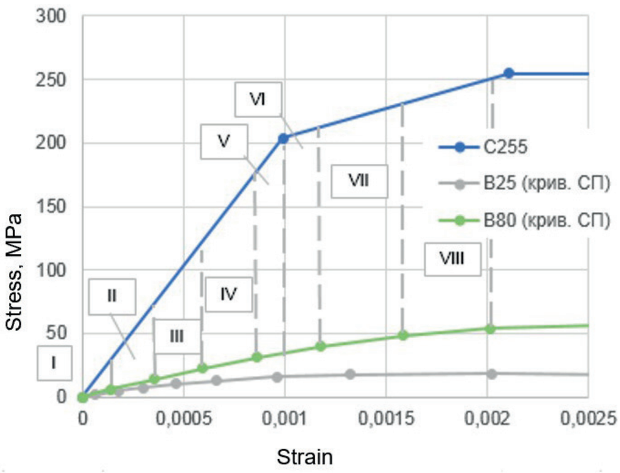

Figure 3. To the description of the stages of steel-reinforced concrete compressed bar performance: combination of three-line diagram for steel and curvilinear diagram for concrete respectively (S3L+BCL)

To verify the solution of this problem, the results of central compression tests of columns with I-beam rigid reinforcement and concrete prisms without reinforcement have been examined. The study of only centrally compressed models, centering of which is performed with special care during the tests, allows us to reliably assess the degree of joint operation of the structure and correctly measure the actual shortening of the models without the effects of buckling at eccentric compression and non-uniform loading of different materials in the cross-section. Models K-3 and K-13 have a nominal cross-sectional dimension of 400x400 mm in concrete, the length of the column model is 1640 mm. The cross section of the steel core is a welded I-beam made of sheet steel C255 according to GOST 27772. Concrete was of compressive strength class B25. Calculated longitudunal reinforcement was of class A400, diameter - 8 mm (8 pcs.). Transverse reinforcement was of class A240, 120 mm spacing, 4 mm diameter. The reinforcement ratio is 10.7%. To provide joint performance of the steel core with concrete it is envisaged to install studs on the walls of the I-beams made of short pieces of reinforcement with diameter of 8 mm, length of 90...120 mm and spacing of about 200 mm. The general view of the steel core and location of the studs is shown in Figure 4, a. Models K10-3, K10-8, K10-11 have smaller concrete cross-sectional dimensions of 150x150 mm. The length of the column model is 600 mm. The steel core is an I-beam made of two channels No.10 reinforced with sheet steel along the wall to achieve a higher ratio of reinforcement. For this purpose, steel C255 according to GOST 27772-88 and concrete of class B80 were used. Working reinforcement was of class A400C; 4 pcs number of bars, 8 mm diameter. Transverse reinforcement was of class A240, 50 mm spacing, 4 mm diameter. The ratio of reinforcement is from 10% to 17.5%. The cross-section is shown in Figure 4, b. In addition to the steel reinforced concrete models, concrete prisms without additional reinforcement were tested with characteristics corresponding to the K10 model group made of B80 concrete. Also, 3 cube specimens with a side of 100 mm were prepared for each concrete casting batch, that is 39 specimens tested in total. The characteristics of the tested models are summarized in Table 1. The calculated shortenings according to formulas 1...5 are given in Table 2 for different curves, the designations of which are adopted in accordance with Figure 1.

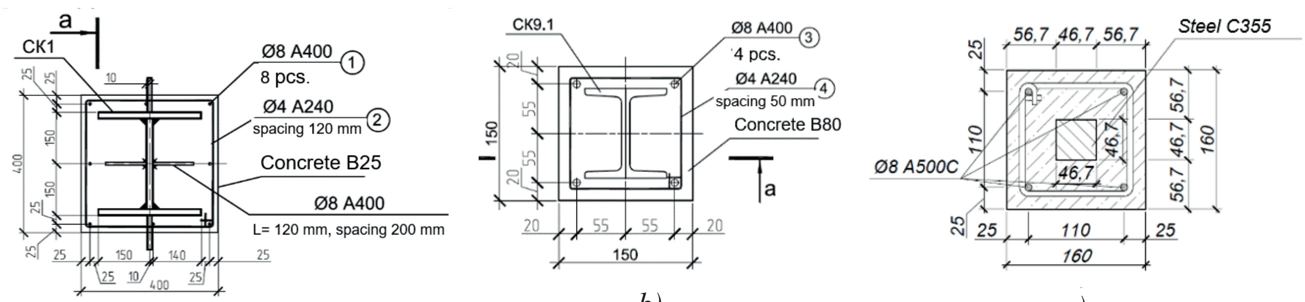

a) b) c)

Figure 4. Tested cross sections: a - K-3, K-13, b - K10-3, K10-8, K10-11, K-9-7, c - SQ type model with square core (FEM only)

Table 1. Parameters of the tested specimens

No	μ, % reinf.	Core steel	Concrete	Additional anchorage of the core	Concrete age at test, days	Compress. Strength of cubes, MPa	h, cm	b, cm	L, cm	Ultimate load N_{ult}, rN		
										Characteristic	FEM	Test (mean)
1	2	3	4	5	6	7	8	9	10	11	12	13
K-3	10.7	C255	B25	+	135	28.55	39.7	39.9	164	6481	6480	6592
K-13	10.7	C255	B25	+	135	28.55	40.0	39.9	164			
K10-3	22.0	C255	B80	-	27	93.8	15.1	15.1	60	2037	2038	2423
K10-8	22.0	C255	B80	-	27	93.8	15.1	15.2	60			
K10-11	22.0	C255	B80	-	94	104.4	15.2	14.9	60			
CP 1	0.0	-	B80	-	90	97.9	15.0	14.9	60	1258	-	1733
CP 2	0.0	-	B80	-	90	97.9	15.0	15.0	60			
CP 3	0.0	-	B80	-	90	97.9	15.0	15.0	60			
SQ	22.0	C255	B80	-	-	-	15.0	15.0	60	2037	2037	-

Notes:
μ is the ratio of reinforcement equal to the ratio of the area of steel in the cross-section to the area of flexible and rigid reinforcement; h, b is the dimensions of the cross-section of the concrete part, L is the length of the specimen, along the axis of which the external load is transferred; N_{ult} is the ultimate load, determined by characteristic values of strength of materials (characteristic), by FE-modeling (FEM), Test - by the results of the experiment.

Table 2. Theoretical shortening according to different diagrams, mm

No	At failure (for ε_{b2})			At appearing of plastic strain in concrete (for ε_{b0})		
	S2L+B3L	S3L+B3L	S3L+BCL	S2L+B3L	S3L+B3L	S3L+BCL
1	2	3	4	5	6	7
K3 K13	5.74	5.74	5.54	3.28	3.28	3.31
K-10-11 K-10-8 K-10-3	1.86	1.86	1.99	1.20	1.20	1.21
CP 1 CP 2 CP 3	1.86		2.75	1.86		1.85
SQ	1.55	1.55	1.31	1.00	1.00	1.01

The tests were carried out using a calibrated hydraulic jack creating axial load up to 1000 tf (10 MN) in the V.A. Kucherenko Central Research Institute for Structural Engineering. Loading was carried out in accordance with GOST 8829-94 “REINFORCED CONCRETE AND PREFABRICATED CONCRETE BUILDING PRODUCTS. Loading test methods. Assesment of strength, rigidity and crack resistance”. According to standard methodic, the load was applied by steps, each step was not more than 10% of the failure load. The endurance for 10 minutes was carried out at each step. When the design (control load) was reached, the endurance was carried out for 30 minutes. Instrument readings were reading continuously at each step of loading with a frequency of 1 Hz. The “central” compression of the model was ensured by centering the column model relative to the marks on the press tables, as well as by monitoring the readings of strain gauges during the first steps of loading. If the corresponding strain gauges showed significant strain differences, the model was additionally aligned to the table. Thus, all the stress non-uniformities arising as a result of the tests at “central” compression in cross-sections are caused only by random internal eccentricities of the model. In the course of the tests under stepwise application of compressive load, the stresses in steel and concrete elements of column models in longitudinal and transverse directions, vertical absolute shortening of the models by means of digital displacement sensors fixed on the upper and lower tables of the press with a measurement accuracy of 0.001 mm were recorded at each step.

Finite element numerical simulation in ATENA PC was performed for models similar in size and material properties, taking into account the nonlinear behavior of materials: curvilinear diagram for concrete and three-linear diagram for steel. The number of steps and mesh size for each model was also selected separately. The minimum number of loading steps was at least 20...30 and the mesh size was about 20 mm. To describe the performance of concrete, the material model Fracture-Plastic Constitutive Model (CC3DCementitious2) was utilized. It is based on the combination of the tensile fracture model with the compressive fracture model of the material. The FE models completely replicated the geometry and mechanical properties of materials of the tested structures as shown in Figure 4 and Table 1. In addition, bars with a square core as shown in Figure 4,c were modeled to verify the effect of cross-sectional shape on concrete performance. Structures with contact interaction between steel and concrete were also modeled. It was found that for models with small or zero eccentricities, the presence of a finite contact interaction at the steel-concrete joint practically does not affect the results of calculations of longitudinal deformations of the column. That is, there is no influence of the contact on the value of the ultimate load and on the value of the ultimate longitudinal deformation of the bar. The difference between forces and deformations for similar models with and without modeling of contact interaction is less than 0.5%. Therefore, the contact interaction at the joint “steel-concrete” was not modeled in a special way, and the finite elements of steel and concrete had common nodes in the calculation scheme. The view of FE models is shown in Figure 5.

Capacity calculation according to the nonlinear deformation model [3] practically does not depend on the type of concrete state diagram to determine the cracking moment M_{crc} and ultimate moment M_{ult} in reinforced concrete eccentrically compressed and bent elements, as shown in [11, 12]. When comparing the results of calculation according to SP 63.13330 and experimental data, the authors of [11] found differences of no more than 7.8% and 6.8% of the above moments, respectively, for different variants of concrete constitutive diagrams.

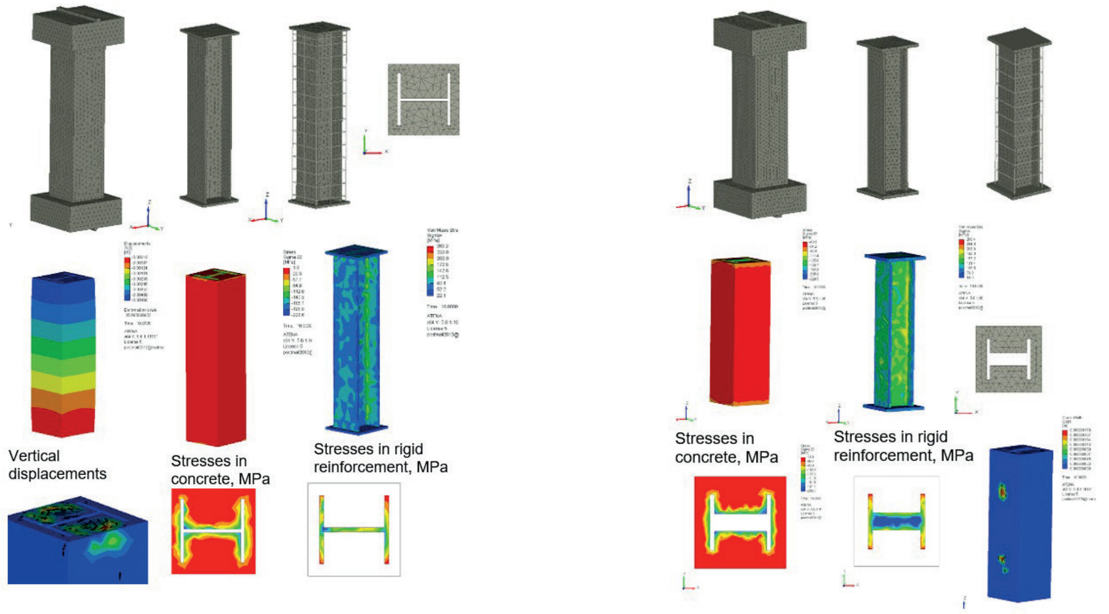

a) b)

Figure 5. FE models: a - model K3; b - model K10-3

RESULTS AND DISCUSSION

The comparative analysis of theoretical, numerical calculations and experimental data on shortening deformations are shown in Figures 6, 7. The comparison of models was performed in the dimensionless coordinate by force, since it is necessary to compare the theoretical calculation, in which the characteristic values of strength and deformation properties of materials are used, and experimental data, in which the values of destructive loads are slightly overestimated relative to the characteristic values. That is, one of the coordinates of the graphs was the value $N/N_{(u,n)}$, where N is the current compressive load in tests or calculations, and $N_{(u,n)}$ is the characteristic ultimate compressive load, which is calculated by the formula:

$$N_{u,n} = R_{bn}A_b + R_{yn}A_{st} + R_{sn}A_s, \quad (6)$$

where R_{bn}, R_{yn}, R_{sn} are the characteristic values of concrete compressive strength, yield strength of steel, design strength of reinforcement, respectively. Thus, the value of $N/N_{u,n}$=1 corresponds to the standard strength of the cross-section ignoring the material and opera-

A. Axial deformations (shortening)

tional condition partial factors. For the tested concrete prisms without reinforcement, $N_{u,n}=R_{bn} A_b$. Also in the plots, horizontal dashed lines show the load level corresponding to the design values of material strength R_b, R_y, R_s calculated by the formula:

$$N_u = R_bA_b + R_yA_{st} + R_sA_s \quad (7).$$

Table 3 summarizes the typical points of the theoretical and experimental curves with each other, and below are figures with strain plots (Figures 6, 7, 8) for the respective models.

Figure 6,a shows the shortening deformations for unreinforced models (concrete prism - CP) made of concrete of compressive strength class B80. In this figure and further gray dashed lines show the experimental data for the same type of models. Blue and green lines respectively indicate theoretical deformations calculated by formulas 1...5, based on three-line and curvilinear diagrams of concrete performance according to SP 63.13330. Fractures of the models during tests occurred with explosive release of energy. It can be seen that the deformation sections from 0 to $N/N_{u,n}$=1.0...1.1 are practically linear.

This corresponds to the actual concrete deformation diagrams obtained by other authors (e.g., [17, 18]) in the section from 0 to the characteristic compressive strength for B80 concrete (R_{bn}=57 MPa; $N_{u,n}$=1). In this case, the actual "straightness" of the experimental curves indicates that a certain margin will be obtained when calculating the shortening strains using the normative curves. At the same time, the curvilinear diagram gives a slightly larger reserve than the three-line diagram at stresses close to the calculated values of concrete strength.

Table 3. Experimental shortenings

No.	Experimental shortening, mm				Shortening by FEM, mm	
	At failure		At the initiation of plastic deformation in concrete		Max	The initiation of plastic deformation in concrete
	For unit test	Mean	For unit test	Mean		
1	2	3	4	5	6	7
K3	6.33	6.24	3.51	3.69	5.16	2.85
K13	6.15		3.87			
K-10-11	2.38	2.17	1.84	1.78	1.68	1.06
K-10-8	2.33		1.81			
K-10-3	1.80		1.68			
CP 1	2.03	1.96	1.40	1.41	-	-
CP 2	2.15		1.51			
CP 3	1.69		1.31			
SQ	-	-	-	-	1.36	1.04

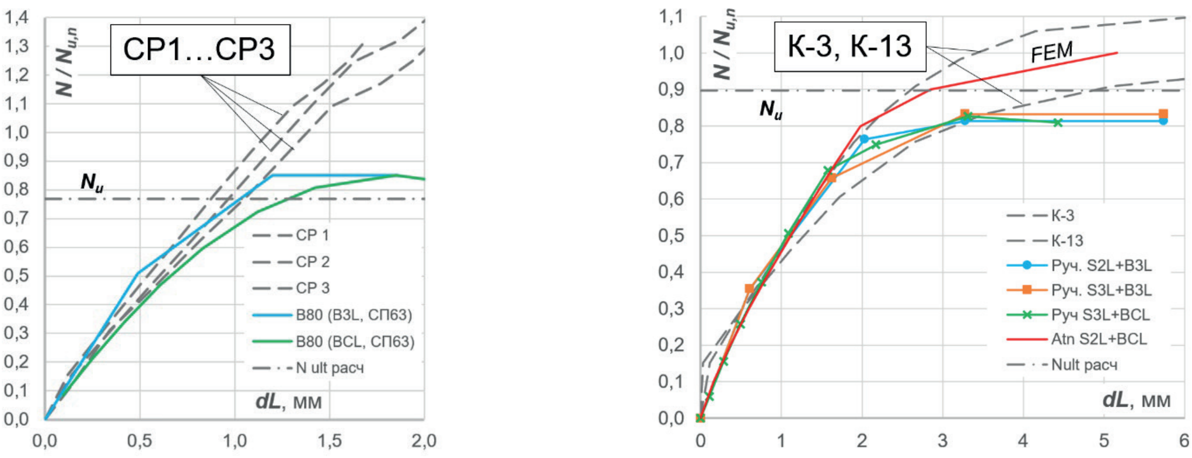

a) b)

Figure 6. Comparison of shortening diagrams: a - concrete models (B80), b - steel reinforced concrete models K3 and K13 (B25)

Figures 6, b and 7 present the shortening strains for the models with rigid reinforcement made of concrete of compressive strength classes B25 and B80 (gray dashed lines). The blue, orange and green lines show the theoretical shortenings determined by formulas 1...5 for various combinations of steel and concrete diagrams. The red line shows the results of FEM analysis utilizing bilinear steel diagram and curvilinear concrete diagram. All theoretical curves follow practically the same trajectory. This circumstance indicates insignificant influence of the diagram type on the linear shortening of the structure.

Experimental shortening curves for the models with concrete B25 have the form of smooth curves (Figure 6, b) with gradually increasing shortening with increasing load. In this case, we can state a good agreement of theoretical assumptions for calculations by formulas 1...5 and by FEM (red solid line).

Models with B80 concrete are shortened according to a slightly different law close to linear (Figure 7), as it was shown above for concrete models without reinforcement (CP) in Figure 6, a. That is, the presence of rigid reinforcement (μ=22%) in the cross-section of the model significantly changes the shortening strain pattern. At load $N/N_{u,n}$=0.5...0.6 the average shortening strain according to the experiment is about 0.85 mm, while the theoretically determined one is about 0.55 mm. At the same time, the values of shortening at load levels $N/N_{u,n}$=0.87, corresponding to the beginning of concrete failure and strains ε_{b0}=0.002, agree with the theoretical values satisfactorily.

Figure 8, a shows a comparison of theoretical and finite element calculations of linear deformations for a structure with a square core. It can be seen that at loads $N/N_{u,n}$=0.7...0.9 the finite element model performs somewhat differently than expected theoretically by formulas 1-5. Comparing the curves obtained by FEM for the structure with I-beam and square cores (Figure 8, b) it can be concluded that the square core operates more efficiently and the structure with it deforms less by about 20-25% at loads close to the calculated values of material strength.

Comparison of experimental results and calculations are summarized in Table 4. Formulas for determining the difference of the compared values are given in the head of the table, where [Teor.] denotes the values calculated by formulas 1...5; [Test] are the values obtained from the results of experiment; [FEM] are the values obtained from the results of FEM simulation.

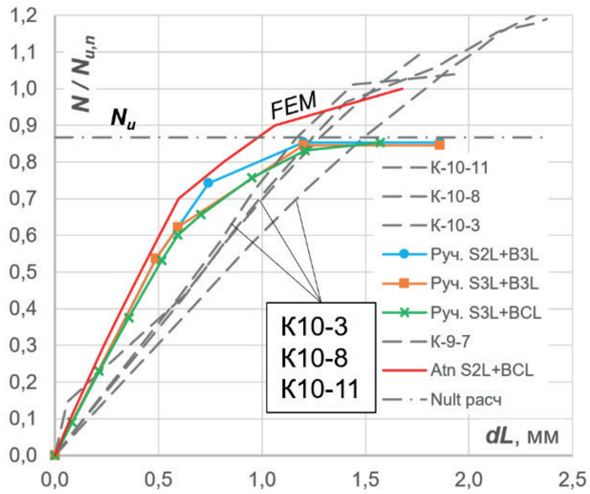

Figure 7. Comparison of shortening diagrams of steel-reinforced concrete models K10 (B80)

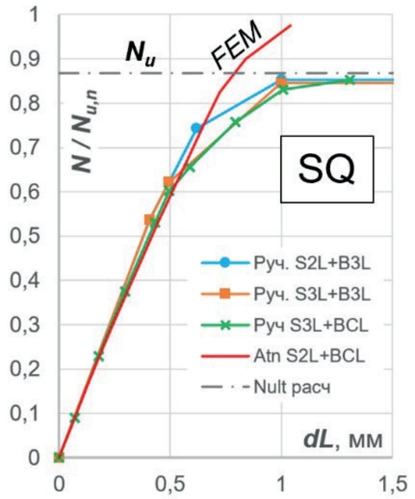

a)

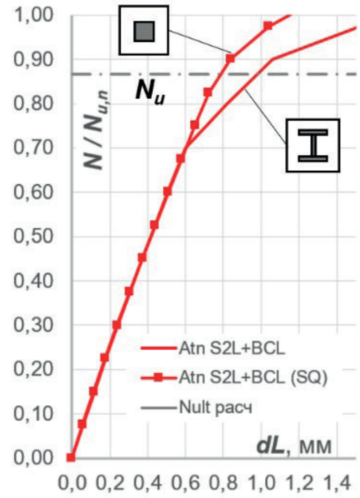

b)

Figure 8. Comparison of shortening diagrams of steel-reinforced concrete models: a - with square core SQ (B80), b - comparison of structure performance with square and I-beam core

It can be seen that the values in columns 2...7 and 8...9 are negative, which means that the calculation of linear shortening deformations using formulas 1...5 or FEM using characteristic diagrams does not provide a reserve relative to the experimental data. That is, if the shortening is calculated according to the standards, underestimated values will be obtained than those obtained by experiment. Thus, the difference for concrete of ordinary strength (type B25) will be 11...17%, and for high-strength it is 14...32%. This circumstance cannot be considered satisfactory. Let's pay attention to the fact that the results of comparison of capacity calculations excluding stability effects with the experiment provide a relatively good convergence and the calculation method according to the formulas of SP 266 or FEM gives the necessary and expected reserve. To illustrate this fact, one can compare the values of columns 11...13 in Table 1.

To eliminate the revealed discrepancy in the value of longitudinal shortening deformation under the action of short-term (short-term, e.g., wind) loads and experimentally obtained data, it is necessary to use a system of additional coefficients. These coefficients should increase the theoretical value of the strains, and should also take into account the peculiarities of concrete of ordinary and high strength as part of compressible steel and reinforced concrete structures. It is established that the following formulas should be used to plot concrete deformation diagrams in accordance with the methodology of SP 63.13330:

$$\varepsilon_{b0(composite)} = 1{,}15\varepsilon_{b0},\ \varepsilon_{b2(composite)} = 1{,}15\varepsilon_{b2} \text{ – for concrete class B25,} \quad (8)$$

$$\varepsilon_{b0(composite)} = 1{,}54\varepsilon_{b0},\ \varepsilon_{b2(composite)} = 1{,}18\varepsilon_{b2} \text{ for concrete of class B80} \quad (9)$$

If the coefficients specified in formulas 8, 9 are used, the necessary reliability and reserve of 2 to 6% for B25 concrete and 1 to 8% for B80 concrete will be realized in structures under short-term loads (see the values in brackets in Table 4). For other intermediate concretes it is allowed to interpolate the presented coefficients by strain values.

Table 4. Comparison of obtained values, %

No.	$\frac{[Teor.]-[Test]}{[Test]}$						$\frac{[FEM]-[Test]}{[Test]}$		$\frac{[Teor.]-[FEM]}{[FEM]}$	
	At failure			At the initiation of plastic deformation of concrete			At failure	At the initiation of plastic deformation of concrete	At failure	At the initiation of plastic deformation of concrete
	Data used									
	Table 2 Table 3	Table 2 Table 3	Table 2 Table 3	Table 2 Table 3	Table 2 Table 3	Table 2 Table 3	Table 3	Table 3	Table 2 Table 3	Table 2 Table 3
	Type of theoretical material deformation curve (S - steel according to SP 16, B - concrete according to SP 63)									
	S2L+ B3L	S3L+ B3L	S3L+ BCL	S2L+ B3L	S3L+ B3L	S3L+ BCL	S3L+ B3L	S3L+ B3L	S3L+ B3L	S3L+ B3L
1	2	3	4	5	6	7	8	9	10	31
K3 K13	-8,0 (5,8)	-8,0 (5,8)	-11,2 (2,1)	-11,2 (2,1)	-11,2 (2,1)	-10,3 (3,1)	-17,3	-22,9	11,3	15,2
K-10-11 K-10-8 K-10-3	-14,2 (0,9)	-14,2 (0,9)	-8,3 (7,9)	-32,6 (3,7)	-32,6 (3,7)	-32,1	-22,6	-40,3	10,8	13,0
CP 1 CP 2 CP 3	-4,9		-	-	-	-	-	-	-	-
SQ	-	-	-	-	-	-	-	-	14,0	-4,0
Note: values in parentheses are given by using the proposed factors for the construction of material deformation diagrams										

B. Axial stiffness of compressed bars

The effective geometric characteristics of the cross-sections must be utilized and the stiffnesses of the elements must be calculated. Due to the active inclusion in spatial performance, including the action of wind loads, it is extremely important to correctly determine the stiffness of the elements when assessing the overall deformation of the building. Based on the results of the conducted experiments, it is possible to estimate the reduced (total) axial stiffness of compressed steel-reinforced concrete structures at each design or loading stage. It is possible to plot the diagram "force vs. axial stiffness" ($N/N_{u,n}$) - $D_{a.i}$) on the basis of the adopted approach of division of diagrams into stages by transforming formulas 4, 5:

$$\Delta D_{a.i} = \frac{\Delta N_i L}{\Delta l_i}\ , \qquad (10)$$

where Δl_i is the shortening according to the results of the experiment at load N_i at the i^{th} stage of loading. The graphs of stiffness variation depending on the applied load are shown in Figures 9...11. On the horizontal axis of the graphs the value $N/N_{u,n}$ is plotted, where N is the current compressive load at tests or calculations, and $N_{u,n}$ is the normative ultimate compressive load, which is calculated according to the formula 6. The vertical dashed line corresponds to the load level corresponding to the design strength values of materials R_b, R_y, R_s, calculated by formula 7. Experimental data are shown in gray dashed lines. Blue, orange, green lines show the theoretical values of stiffnesses according to formula 10. Red line shows the stiffness of the compressed structure according to the numerical model. The horizontal black dashed line on the graphs shows the value of the reduced normative axial stiffness of the section $D_{a,n}$, calculated by the formula similar to G.11 of SP 266.1325800, where instead of the moment of inertia the cross-sectional areas are taken, and the coefficients k_s=k_b=1 and the concrete deformation modulus - E_{b1}=0.85E_b, as under short-term load action.

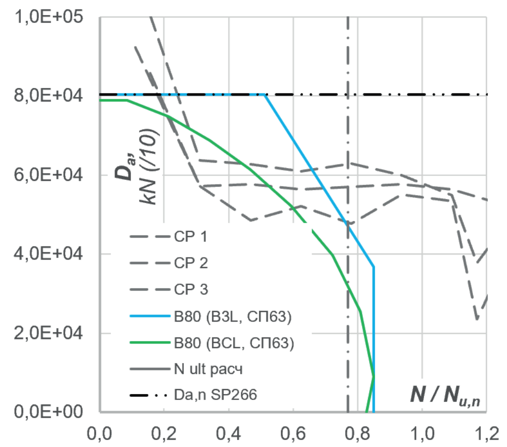

Figure 9. Diagrams of change in stiffness D_a as a function of load for concrete models (B80)

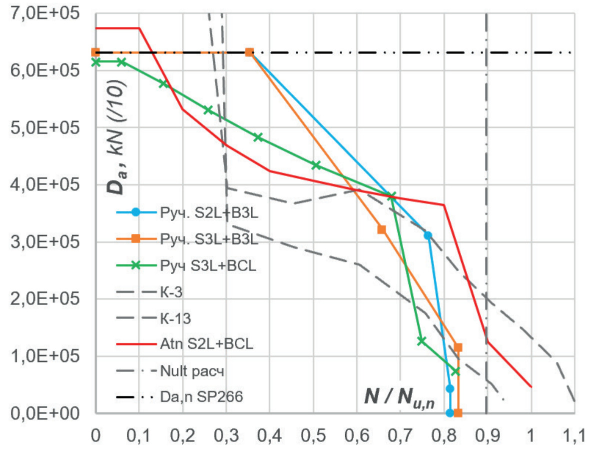

Figure 10. Diagrams of change in stiffness D_a as a function of load for steel reinforced concrete models K3 and K13 (B25)

The stiffness of unreinforced models (concrete prisms CP1...CP3 - gray dashed line in Figure 9) at the initial stages of loading of structures (at $N/N_{u,n}$=0...0.3) is much higher than the value of $D_{a,n}$. Further, after initial compression, the stiffness begins to drop to a value of about 0.75$D_{a,n}$ and remains stable up to a load of about $N/N_{u,n}$=1.1. The stiffness graph goes sharply downward to a value of about 0.4...0.5$D_{a,n}$. Failure ($D_{a,n}$=0) occurs at about the load level $N/N_{u,n}$=1.4. The utilization of nonlinear strain diagrams will allow a fairly accurate modeling of the behavior of concrete under load and the graph shows that the curvilinear diagram is obviously more accurate in describing the performance of concrete under load (green line), compared to the tri-linear diagram (blue line).

The stiffness of steel-reinforced concrete models made of B25 concrete (gray dashed line in Figure 10) at the initial stages of structural loading (at $N/N_{u,n}$=0...0.3) is much higher than the value of $D_{a,n}$. Further, after the initial compression, the stiffness starts to drop sharply to a value of about 0.56$D_{a,n}$. At the load range $N/N_{u,n}$=0.3...1.05 it steadily decreases almost to 0. Failure ($D_{a,n}$=0) occurs approximately at the load level $N/N_{u,n}$=1.07. The comparison shows that the use of the curvilinear diagram also shows a good convergence with the experimental curves (green line), while the three-line diagram of concrete and steel (orange) and even more so the two-line diagram (blue) give an unjustified overestimation of the stiffness at loads $N/N_{u,n}$=0...0.5. Numerical modeling using the curvilinear concrete deformation diagram (red line) also shows a good convergence with the experimental stiffness diagram.

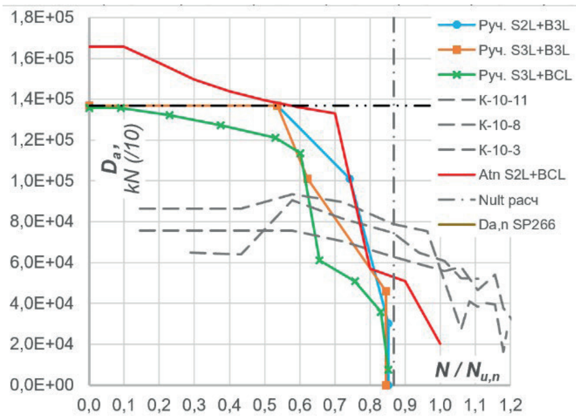

Figure 11. Diagrams of change in stiffness D_a as a function of load for steel-reinforced concrete models K10 (B80)

The stiffness of steel-reinforced concrete models made of B80 concrete (gray dashed line in Figure 11) at the initial stages of loading of the structures (at $N/N_{u,n}$=0...0.3), as well as for the above considered models, is significantly higher than the value of $D_{a,n}$. Further, after the initial compression, the stiffness begins to drop to a value of about $0.57D_{a,n}$ and remains stable up to a load of about $N/N_{u,n}$=0.7. After the plastic deformations start to develop in the steel core at the load range $N/N_{u,n}$=0.7...1.2 the stiffness of the element decreases smoothly to the value of $0.3D_{a,n}$. Here cracks actively develop and separation of concrete from steel takes place and the stiffness diagram sharply goes down to the value of about $0.14D_{a,n}$. Failure ($D_{a,n}$=0) occurs at approximately the load level $N/N_{u,n}$=1.4. It can be seen that the diagram of stiffness change in steel-reinforced concrete structure made of high-strength concrete (B80) and with high ratio of reinforcement (model type K10) practically repeats the diagram for unreinforced concrete (Figure 9). There are the same characteristic steps of stiffness drop and then a stable stiffness value without significant decrease over the load range $N/N_{u,n}$=0.3...0.7. At the same time, modeling of stiffness by formulas 4, 5, 10 (orange line), as well as by the finite element method (red) using curvilinear diagram of concrete deformation and three-linear diagram for steel do not provide an accurate description of the change of stiffness (as well as deformation) of the structure in the range of loads $N/N_{u,n}$=0.3...0.7.

In order to bring the axial stiffness to a value close to the experimental data, it is proposed to introduce an additional coefficient $k_{composite}$ in accordance with Formula 11, Table 5 and Figure 12 when calculating stiffnesses for steel-reinforced concrete structures under the action of short-term loads:

$$D_{a,composite} = k_{composite}(0.85E_bA_b + E_sA_s + E_{st}A_{st}), \quad (11)$$

Table 5. Correction factor to modulus of deformation

$N/N_{u,n}$	$k_{composite}$ for steel reinforced concrete structures with reinforcement ratio μ≤22% and heavy concrete of compressive strength class	
	B25	B80
1	2	3
0	1	1
0.3	0.55	0.55
0.7	-	0.55
1	0.1	0.3
1	0	0

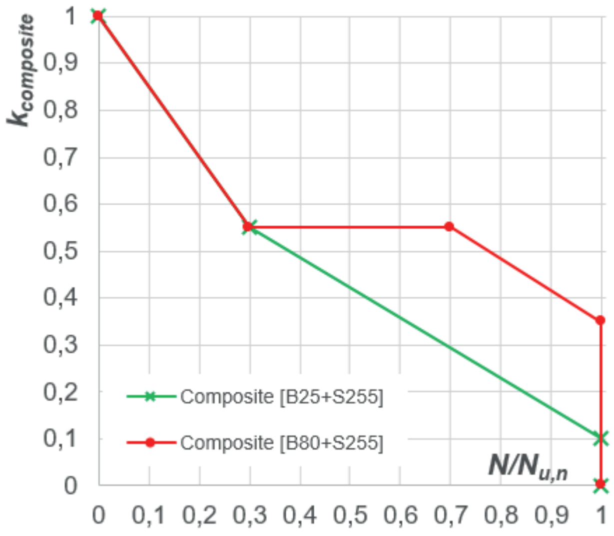

Figure 12. Diagram if the coefficient $k_{composite}$

CONCLUSION

1. Longitudinal shortening deformations for steel-reinforced concrete compressed members have been evaluated with a wide range of heavy concretes (from B25 to B80) and reinforcement ratios (from 0 to 22%). Deformations were calculated manually using modified formulas of SP 63.13330 taking into account three types of concrete deformation diagrams (two- and three-line, curvilinear) and two types of steel deformation diagrams (two- and three-line according to SP 16.13330). Finite element method analysis of structural models has been performed. These calculations take into account the characteristic diagrams of materials performance, as well as the possibility of slippage at the steel-concrete contact in accordance with [4]. Experimental data obtained during testing of conditionally centrally compressed column models of steel-reinforced concrete structures have been analyzed.
2. It has been found that the existing concrete performance diagrams do not accurately describe the performance of a composite steel-reinforced concrete structure, namely its shortening and reduced stiffness. When the concrete structure operates in compression, its failure at earlier stages of loading than it would be for concrete or reinforced concrete. This circumstance is due to the stress-strain state of the concrete section separated by steel elements, as well as to the effects of early delamination and slippage on the steel-concrete contact surface.
3. To eliminate the identified discrepancy in determining the value of longitudinal deformation (shortening) under the action of short-term loads and experimentally obtained data, it is necessary to use a system of additional coefficients. These coefficients should increase the theoretical value of the expected strains ε_{b0} and ε_{b2}, and should also account for the peculiarities of the operation of concrete of ordinary and high strength as part of compressible steel and reinforced concrete structures.
4. To bring the calculated axial stiffness to a value close to the experimental data, it is suggested to introduce an additional coefficient $k_{composite}$, which additionally reduces the axial stiffness of the structure depending on the level of stresses in concrete and steel, when calculating the stiffness values for steel-reinforced concrete structures under the action of short-term loads.
5. Considering the curvilinear diagram of concrete in compression provides more accurate results of the serviceability limit state (for deformations) than two- and three-line diagrams when performing calculations of spatial schemes of complex structures taking into ac-

count physical nonlinearity on the deformed scheme. Curvilinear diagrams more accurately describe the deformations of the structure operating in compression at the initial stages of deformation and loading.

REFERENCES

1. ANSI/AISC 360-16 An American National Standard. Specification for Structural Steel Buldings. (2016) Chicago: American Institute of Steel Construction. 676 p.
2. **Griffis, L.G.** (1993) Serviceability Limit States Under Wind Load. *Engineering Journal. American Institute of Steel Construction*. Q1. pp. 1-16.
3. **Travush V.I., Konin D.V., Rozhkova L.S., Krylov A.S., Kaprielov S.S., Chilin I.A., Fimkin A.I** (2016) Eksperimental'nye issledovaniya stalezhelezobetonnyh konstrukcij, rabotayushchih na vnecentrennoe szhatie [Experimental studies of steel-reinforced concrete structures operating on off-center compression]. *Academia. Architecture and construction*, no 3, pp. 127-135.
4. **Travush V.I., Kaprielov S.S., Konin D.V., Krylov A.S., Kashevarova G.G., Chilin I.A** (2016) Opredelenie nesushchej sposobnosti na sdvig kontaktnoj poverhnosti «stal'-beton» v stalezhelezobetonnyh konstrukciyah dlya betonov razlichnoj prochnosti na szhatie i fibrobetona [Determination of the bearing capacity for shear of the contact surface "steel-concrete" in steel-reinforced concrete structures for concretes of various compressive strength and fiber concrete]. *Construction and reconstruction*, no 4 (66), pp. 45-55.
5. **Desyatkin M.A., Konin D.V., Martirosyan A.S., Travush V.I**. (2015) Raschet stalezhelezobetonnoj kolonny vysotnogo doma na kosoe vnecentrennoe szhatie [Calculation of a steel-reinforced column of a high-rise building for oblique off-center compression] *Housing construction,* no 5, pp. 92-95.
6. **Travush V.I., Rozhkova L.S., Krylov A.S.** (2016) Otechestvennyj i zarubezhnyj opyt issledovanij raboty stalezhelezobetonnyh konstrukcij na vnecentrennoe szhatie [Domestic and foreign experience in researching the operation of steel-reinforced concrete structures for non-central compression] *Construction and reconstruction,* no 5, pp. 31-44.
7. **Mukhamediev T.A., Starchikova O.I.** (2016) Raschet prochnosti stalezhelezobetonnyh kolonn s ispol'zovaniem deformacionnoj modeli [Calculation of the strength of steel-reinforced concrete columns using a deformation model] *Concrete and reinforced concrete*, no 4, pp. 18-21.
8. **Karpenko N.I.** (1996) Obshchie modeli mekhaniki zhelezobetona [General models of reinforced concrete mechanics] Moscow: Stroyizdat, 416 p. (In Russian)
9. **Murashkin G.V., Murashkin V.G.** (1997) Modelirovanie diagrammy deformirovaniya betona i skhemy napryazhenno-deformirovannogo sostoyaniya [Modeling of the deformation diagram of concrete and the scheme of the stress-strain state] *Izvestiya vysshih uchebnyh zavedenij. Stroitel'stvo*, no 10, pp. 4-6.
10. **Mordovsky S.S., Murashkin V.G.** (2012) Napryazhyonnoe sostoyanie eksperimental'nyh obrazcov pri vnecentrennom nagruzhenii [The stressed state of experimental samples under extreme loading]. *Sovremennye problemy nauki i obrazovaniya,* no 4. Available at: http://science-education.ru/ru/article/view?id=6794 (accessed 03 January 2018).
11. **Karpenko N.I., Sokolov B.S., Radaykin O.V**. (2013) K raschyotu prochnosti, zhyostkosti i treshchinostojkosti vnecentrenno szhatyh zhelezobetonnyh elementov s primeneniem nelinejnoj deformacionnoj modeli [On the calculation of strength, stiffness and crack resistance of non-centrally compressed reinforced concrete elements using a nonlinear deformation model]. *Izvestiya Kazanskogo gosudar-*

stvennogo arhitekturno-stroitel'nogo universiteta, no 4(26), pp. 113-120.

12. **Karpenko N.I., Karpenko S.N.** (2012) O diagrammnoj metodike rascheta deformacij sterzhnevyh elementov i ee chastnyh sluchayah [On the diagrammatic methodology for calculating deformations of rod elements and its special cases] *Concrete and iron-concrete*, no 6, pp. 20-27.
13. **Arleninov P.D.** (2016) Deformation and stability of compressed and non-centrally compressed core reinforced concrete elements, taking into account creep and cracking (PhD thesis), Moscow, JSC "SIC "Construction" (NIIZHB named after A.A. Gvozdev). – 143 p. (In Russian)
14. **Krylov S.B.** (2012) Kriticheskaya sila dlya zhelezobetonnyh sterzhnevyh elementov [Critical force for reinforced concrete core elements] *Academia. Architecture and Construction*, no 2, pp. 136-138.
15. **Arleninov P.D.** (2015) Analiz razlichnyh metodik sozdaniya raschetnyh skhem pri komp'yuternom modelirovanii nesushchih konstrukcij [Analysis of various methods for creating computational schemes for computer modeling of load-bearing structures] *BST: Byulleten' stroitel'noj tekhniki*, no 5(969), pp.58-59.
16. **Karpenko N.I., Sokolov B.S., Radaykin O.V.** (2013) Analiz i sovershenstvovanie krivolinejnyh diagramm deformirovaniya betona dlya rascheta zhelezobetonnyh konstrukcij po deformacionnoj modeli [Analysis and improvement of curvilinear diagrams of concrete deformation for the calculation of reinforced concrete structures according to the deformation model] *Industrial and civil construction*, no.1, pp.28-30.
17. **Bezgodov, I., Kaprielov, S., & Sheynfeld, A.** (2022) Relationship between strength and deformation characteristics of high-strength self-compacting concrete. *International Journal for Computational Civil and Structural Engineering*, no 18(2), pp. 175–183.
18. **Kaprielov, S., Sheinfeld, A., Selyutin, N.** (2022) Control of heavy concrete characteristics affecting structural stiffness. *International Journal for Computational Civil and Structural Engineering*, no18(1), pp. 24–39.
19. **Chiorino M.A., Carreira J.** (2012) Factors Affecting Creep and Shrinkage of Hardened Concrete and Guide for Modelling. *The Indian Concrete Journal,* no 12(86), pp.11-24.
20. **Guilin Zhang, Pang Chen, Xiaoyu Si, Jingde Wang, Yang Han** (2022) Research on Shrinkage and Shrinkage Models of Reinforced Concrete Specimens. *The Open Civil Engineering Journal*, no 16(1), pp. 1-10.
21. **Darko Nakov** (2024) Early-age thermal and shrinkage cracking in reinforced concrete structures. Proceedings of the *Contemporary Civil Engineering Practice 2024*, *June 2024, Ruma, Serbia*, pp. 40-51.

СПИСОК ЛИТЕРАТУРЫ

1. ANSI/AISC 360-16 An American National Standard. Specification for Structural Steel Buldings. – Chicago: American Institute of Steel Construction. 2016. 676 p.
2. **Griffis, L.G.** Serviceability Limit States Under Wind Load // Engineering Journal. American Institute Of Steel Construction, 1993, Q1. pp. 1-16.
3. **Травуш В.И., Конин Д.В., Рожкова Л.С., Крылов А.С., Каприелов С.С., Чилин И.А., Фимкин А.И.** Экспериментальные исследования сталежелезобетонных конструкций, работающих на внецентренное сжатие // Academia. Архитектура и строительство. 2016, № 3, С. 127-135.
4. **Травуш В.И., Каприелов С.С., Конин Д.В., Крылов А.С., Кашеварова Г.Г., Чилин И.А.** Определение несущей способности на сдвиг контактной поверхности «сталь-бетон» в сталежелезобетонных конструкциях для бетонов различной прочности на сжатие и фибробетона // Строительство и реконструкция, 2016, №4 (66), С. 45-55.

5. **Десяткин М.А., Конин Д.В., Мартиросян А.С., Травуш В.И.** Расчет сталежелезобетонной колонны высотного дома на косое внецентренное сжатие // Жилищное строительство, 2015, № 5, С. 92-95.
6. **Травуш В.И., Рожкова Л.С., Крылов А.С.** Отечественный и зарубежный опыт исследований работы сталежелезобетонных конструкций на внецентренное сжатие // Строительство и реконструкция, 2016, №5, С. 31-44.
7. **Мухамедиев Т.А., Старчикова О.И.** Расчет прочности сталежелезобетонных колонн с использованием деформационной модели // Бетон и железобетон, 2006, №4, С. 18-21.
8. **Карпенко Н.И.** Общие модели механики железобетона. – М.: Стройиздат, 1996. – 416 с.
9. **Мурашкин Г.В., Мурашкин В.Г**. Моделирование диаграммы деформирования бетона и схемы напряженно-деформированного состояния // Известия высших учебных заведений. Строительство, 1997, №10, С. 4-6.
10. **Мордовский С.С., Мурашкин В.Г.** Напряжённое состояние экспериментальных образцов при внецентренном нагружении // Современные проблемы науки и образования, 2012, № 4. URL: http://science-education.ru/ru/article/view?id=6794 (дата обращения: 01.03.2018).
11. **Карпенко Н.И., Соколов Б.С., Радайкин О.В.** К расчёту прочности, жёсткости и трещиностойкости внецентренно сжатых железобетонных элементов с применением нелинейной деформационной модели // Известия Казанского государственного архитектурно-строительного университета, 2013, №4(26), С. 113-120.
12. **Карпенко Н.И., Карпенко С.Н.** О диаграммной методике расчета деформаций стержневых элементов и ее частных случаях // Бетон и железобетон, 2012, №6, С. 20-27.
13. **Арленинов П.Д.** Деформирование и устойчивость сжатых и внецентренно сжатых стержневых железобетонных элементов с учетом ползучести и трещинообразования – Кандидатская диссертация, АО «НИЦ «Строительство» (НИИЖБ им. А.А. Гвоздева), 2016, С. 143.
14. **Крылов С.Б.** Критическая сила для железобетонных стержневых элементов // Academia. Архитектура и строительство, 2012, №2, С. 136-138.
15. **Арленинов П.Д.** Анализ различных методик создания расчетных схем при компьютерном моделировании несущих конструкций // БСТ: Бюллетень строительной техники, №5(969), 2015, С.58-59.
16. **Карпенко Н.И., Соколов Б.С., Радайкин О.В.** Анализ и совершенствование криволинейных диаграмм деформирования бетона для расчета железобетонных конструкций по деформационной модели // Промышленное и гражданское строительство, 2013, №1, С.28-30.
17. **Bezgodov, I., Kaprielov, S., & Sheynfeld, A.** Relationship between strength and deformation characteristics of high-strength self-compacting concrete // International Journal for Computational Civil and Structural Engineering, 2022, №18(2), pp. 175–183.
18. **Kaprielov, S., Sheinfeld, A., Selyutin, N.** Control of heavy concrete characteristics affecting structural stiffness // International Journal for Computational Civil and Structural Engineering, 2022, №18(1), pp. 24–39.
19. **Chiorino M.A., Carreira J.** Factors Affecting Creep and Shrinkage of Hardened Concrete and Guide for Modelling // The Indian Concrete Journal, 2012, № 12(86), pp. 11-24.
20. **Guilin Zhang, Pang Chen, Xiaoyu Si, Jingde Wang, Yang Han**. Research on Shrinkage and Shrinkage Models of Reinforced Concrete Specimens // The Open Civil Engineering Journal, 2022, no 16(1), pp. 1-10.

21. **Darko Nakov.** Prsline usled rane termičke kontrakcije i skupljanja u armirano-betonskimkonstrukcijama // Proceedings of the Contemporary Civil Engineering Practice 2024, 2024, Ruma, Serbia, pp. 40-51.

Denis Vladimirovich Konin - PhD, deputy director for scientific work Research Institute of Building Constructions (TSNIISK) named after V. A. Koucherenko JSC Research Center of Construction: 6, 2nd Institutskaya street, Moscow, 109428, Russia; konden@inbox.ru

Денис Владимирович Конин - кандидат технических наук, заместитель директора по научной работе Центрального научно-исследовательского института строительных конструкций (ЦНИИСК) им. В.А. Кучеренко АО «Научно-исследовательский центр (НИЦ) «Строительство»): д. 6, 2-я Институтская ул., г. Москва, 109428, Россия; konden@inbox.ru